Building and Environment 85 (2015) 220–232

Contents lists available at ScienceDirect

Building and Environment

journal homepage: www.elsevier.com/locate/buildenv

Basement radon entry and stack driven moisture infiltration reduced by active soil depressurization

C.R. Boardman*, Samuel V. Glass

Forest Products Laboratory, U.S. Forest Service, 1 Gifford Pinchot Dr., Madison, WI 53726, USA

ARTICLE INFO

Article history:
Received 15 September 2014
Received in revised form
24 November 2014
Accepted 6 December 2014
Available online 16 December 2014

Keywords:
Radon
Moisture
Soil gas
Stack effect
Active soil depressurization
Permanent wood foundation

ABSTRACT

This case study presents measurements of radon and moisture infiltration from soil gases into the basement of an unoccupied research house in Madison, Wisconsin, over two full years. The basement floor and exterior walls were constructed with preservative-treated lumber and plywood. In addition to continuous radon monitoring, measurements included building air tightness, indoor–outdoor pressure difference, indoor and outdoor temperature and relative humidity, wood moisture content, and tracer gas decay. A single-zone air infiltration model was calibrated based on tracer gas measurements. Soil moisture infiltration was determined by mass conservation after accounting for all other moisture flows: humidification, air exchange, diffusion through the above-grade building envelope, sorption in hygroscopic materials, and moisture removal by air conditioning. A moisture balance methodology used in previous work was validated and improved here by including two time scales in the sorption modeling. Active soil depressurization was applied and shown to reduce both radon and soil moisture infiltration. The stack effect is shown to correlate well with soil moisture infiltration but does not fully explain radon entry.

Published by Elsevier Ltd.

1. Introduction

Soil gases entering the indoor environment can have a significant impact on indoor air quality. There are a variety of concerns and assessment models for indoor environmental quality [1], but interest in indoor air pollutants, specifically Volatile Organic Compounds (VOCs) and Radon, is long-standing [2–4]. This study focuses on the neglected topic of soil moisture infiltration which affects not only occupant health, but also building durability [5]. In previous work a moisture balance model was developed to estimate the rate of moisture infiltration from soil surrounding a basement foundation, and that rate was shown to correlate with stack effect driven air exchange for the research and demonstration house on the campus of the Forest Products Laboratory (FPL) in Madison, WI [6]. The current study was prompted by the realization that radon was also entering this house. Active sub-slab depressurization has long been recognized as an effective method for radon reduction if the equipment is properly maintained [7]. Installation of that equipment provided an opportunity to extend research into the effects of active soil depressurization (ASD) on soil moisture entry, thus adding to the case studies explored by Turk and Hughes [8] and recommended by Cheple and Huelman [5].

The early studies which established the effectiveness of ASD for radon mitigation investigated a wide variety of environmental parameters which affect radon entry [9], and identified stack effect, wind pressure, and operation of mechanical ventilation as dominate drivers for radon entry. The review by Gadgil [10] identifies convective entry of radon from soil gas driven by pressure differences as the primary radon entry mechanism in single-family homes and evaluates a variety of models for understanding the driving mechanisms. The case studies by Turk et al. [11] document effectiveness of a variety of radon control techniques including ASD. The extensive modeling done by Krylov and Ferguson [12] identified the large effects wind pressure can have on driving contamination of indoor air by soil gases. Similar wind effects were documented in the case study by Keskikuru et al. [13]. There is still significant interest in understanding the variety of factors which influence vapor intrusion, as reflected for example in the recent study of crack entry by Yao et al. [14].

Although the case study described here provides further data that could help confirm mechanisms for radon entry, the focus is on soil moisture infiltration. The original moisture balance model which is used, extended, and validated in this study was part of a project to better characterize moisture sources in buildings.

* Corresponding author. Tel.: +1 608 231 9227.
E-mail address: cboardman@fs.fed.us (C.R. Boardman).

http://dx.doi.org/10.1016/j.buildenv.2014.12.008
0360-1323/Published by Elsevier Ltd.

Hygrothermal analysis of building envelope assemblies relies on having realistic boundary conditions, and simulation results often depend strongly on the assumed interior humidity levels [15,16]. Lu [17] and Kalamees et al. [18] have shown that indoor moisture generation rates are critical for understanding indoor relative humidity levels. Moisture release from foundations is known to be a potentially large source but is currently poorly characterized [19,20]. Recent work [21] continues to quantify various moisture sources. Moisture buffering by hygroscopic indoor materials also continues to be an area of active research [22,23] which influences indoor relative humidity.

This case study validates the model used to quantify the foundation as a significant moisture source in the FPL research and demonstration house. We specifically test the hypothesis that the moisture balance model should show a significant reduction in soil moisture infiltration in this house when the ASD system is active, mirroring the expected reduction in radon infiltration. This study is thus an extension of the previous work on the FPL research and demonstration house, adding another year of moisture data and adding new measurements of radon levels, pressure differences, and interior wood moisture content. It differs from the case studies further analyzed by Turk [24] in that this is a permanent wood foundation and the basement was a significant moisture source. It also improves the previous moisture balance model by extending the simple moisture buffering model without resorting to modeling of interzonal airflows or more detailed descriptions of moisture buffering [25–27].

2. Experimental methods

2.1. Building description

The test house is a two-story wood-frame building built in 2001 on a permanent wood foundation. Details on the history and performance of the house can be found in Carll et al. [28,29] and Boardman et al [6]. Instead of a concrete slab, the basement floor and walls are constructed from plywood and lumber pressure treated with Chromated Copper Arsenate (CCA). Fig. 1 shows a schematic of the floor and wall detail. Carpet covers approximately 30% of the plywood floor sheathing area in the basement; the remainder is plywood with no covering. The polyethylene sheeting on top of the gravel and under the floor joists was installed to reduce moisture transfer from soil to building by diffusion, but it was not air sealed at the overlaps or perimeter, so transport by convection through gaps or rips in the sheet can occur. Similarly the sheeting covering the exterior of the plywood walls directs bulk rain water away from the foundation and reduces vapor diffusion but is not air sealed.

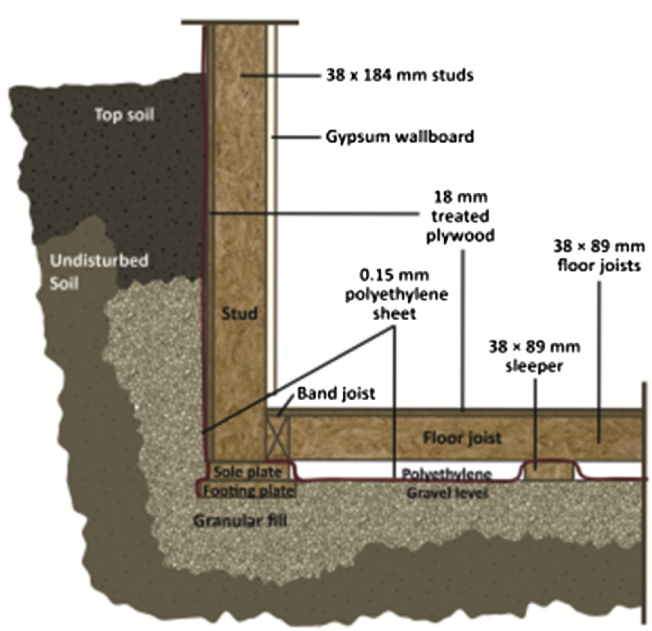

Fig. 1. Test house basement floor and wall detail.

Permanent wood foundations are rare, but the experimental methods, modeling, and certain results from this case study are applicable to more common types of foundation. The moisture balance methodology and models for buffering will work with any foundation. Similarly the stack effect and influence of wind on soil gas entry are general. The specific tuning of the models will reflect the actual air leakage paths and high moisture buffering capacity of this particular house.

2.2. Radon measurement

Initial testing for presence of radon in the basement of the test house was done with alpha track test kits (AccuStar Labs, Medway, MA) over a period of 3.5 months. Subsequently, radon measurements were taken hourly using a continuous radon monitor (RadStar RS800, RadonAway, Ward Hill, MA), which is accurate to ±5% with sensitivity of 0.4 counts per minute per pCi/L. These readings were supplemented with a less sensitive RadStar RS300 (accurate to ±10%) which was moved between indoors and outdoors as needed. Radon remediation, which also affected the moisture infiltration, was done through ASD. The plywood floor joints were sealed with caulk and polyurethane foam was used to seal around water supply and drain openings in order to reduce indoor air loss to the radon exhaust fan. Typical of most radon remediation installations, the exhaust fan was installed outside with rigid PVC pipe connecting to a suction point in the gravel bed below the flooring near the center of the basement. The fan was the same size as typically used for concrete foundations and performed well creating an approximately 125 Pa local depressurization where the pipe first connects to the gravel bed. The pressure field rapidly drops off away from this point due to resistance to air flow through the gravel bed. To verify depressurization far from the fan, two measurements of pressure difference across the plywood floor were made on opposite sides of the basement. One 8.5 m from the fan showed a 3.4 Pa depressurization under the floor, and the other 3 m from the fan showed a 4.6 Pa depressurization. The fan was put on a switch so it could be turned off to resume influx of radon and moisture into the basement.

2.3. Fan flow measurement

A series of blower door tests were run [30], with the radon fan both on and off, to characterize the air tightness of the house under a variety of conditions and begin to quantify the effect of the radon fan on indoor air leakage. An automated system (Minneapolis Blower Door, The Energy Conservatory, Minneapolis, MN) was used to depressurize the house and measure the air flow under the two conditions.

2.4. Pressure and wind speed measurement

A digital pressure and flow gauge (DG-700, The Energy Conservatory, Minneapolis, MN) was also used to monitor the pressure difference between the basement and outdoors. The basement pressure tap was near the floor along the south wall of the basement, while the outdoor tap followed a dryer vent to exit the south wall outside about 1 m above ground level. That tap pointed down to avoid rain entry and was somewhat shielded from the west wind by a corner of the house, but generally exposed to south and east winds. An automated program read and stored the pressure sensor reading every 15 min during the course of this study, with an automatic zero calibration check done before each reading to allow accurate determination of the pressure difference down to 0.1 Pa. Previous investigation had shown that furnace operation had little influence on indoor to outdoor pressure differences [28]. The wind speed was measured on site at roof peak with an ultrasonic anemometer (Gill Instruments Windsonic) with data taken every second but averaged to get a representative hourly value.

2.5. Moisture and temperature measurement

Indoor and outdoor temperature and relative humidity (RH) readings were taken hourly using a Vaisala HMP233 sensor accurate to ±0.2 °C and ±1.0% RH. For this study the wood moisture content (MC) at two locations in the basement was read using moisture pins. One location was in a nominal 2″ × 4″ (38 × 88 mm) wood stud[1] and the other in the plywood floor, both located near the center of the basement. An automated program read and stored the MC as read by a Delmhorst K-1100 In-Kiln Moisture Monitoring System, and readings were checked with a handheld Delmhorst model J-2000, both instruments set to room temperature (70 °F) and southern yellow pine species correction. The raw plywood MC readings were then corrected to give a more accurate moisture content reading following the procedure in Boardman et al. [31], and using the equations for CCA treated plywood in Carll et al. [28].

2.6. Tracer gas measurement

Tracer gas testing allowed quantification of air exchange rates (AERs) in the house. For this study AERs were measured on over 20 individual days, about half with the radon fan on, and half with the fan off. The tracer gas technique utilized sulfur hexafluoride (SF_6) as the tracer gas; tracer gas concentration was determined by electron capture detector gas chromatography. AERs were determined by monitoring decay in the concentrations of tracer gas [32] over the course of eight hours. AERs were usually below 0.2 h^{-1}. The interval between measurements was typically 30 min, with 15 or more readings taken to allow multiple decay time periods to elapse. The furnace fan was set to run continuously during tracer gas tests, and freestanding "box" fans were placed on each floor level to promote even distribution of the tracer gas. Tracer gas concentration was sampled on each floor of the house. The measurement equipment contains internal software that can calculate AER based on all concentration readings. This value was compared to values calculated for each sample location using the simple decay model:

$$C\left(t\right) = C_i e^{-\lambda t} \tag{1}$$

where λ is the decay constant, equivalent to the AER (h^{-1}), t is time since start (h), C_i is initial SF_6 concentration (typically in ppb), and C(t) is SF_6 concentration at time t.

The air exchange rate is then calculated from:

$$\lambda = \frac{1}{t}\ln\left(\frac{C_i}{C(t)}\right) \tag{2}$$

[1] Part of the stairway framing; the moisture pin was 1 m above the floor.

3. Air exchange modeling

3.1. Natural air exchange

Tracer gas data was used to calibrate the Alberta air infiltration model (AIM-2) [33]. AIM-2 is a simple single-zone model for predicting building air infiltration. It was used successfully by Wang et al. [34] to predict natural air exchange in a sample of single-family houses. Some of the core equations are outlined here so that data input values can be understood. The AIM-2 model relies on the indoor–outdoor temperature difference and wind speed to predict infiltration driven by the stack effect and by wind; it also relies on house characteristics that can be derived from a blower door test [30] and estimates of the location of envelope air leakage. Blower door measurements are fit to $Q = C(\Delta P)^n$ where Q is the air leakage flow (m^3/s) due to the pressure difference ΔP (Pa) across the house envelope, C is a flow coefficient ($m^3 s^{-1}\ Pa^{-n}$), and n is a dimensionless exponent. The total air infiltration rate, Q_{aim} (m^3/s), is the sum of the infiltration rate from stack effect, Q_s (m^3/s), and infiltration rate from wind, Q_w (m^3/s), as calculated in Equation (3).

$$Q_{aim} = \left[Q_s^{1/n} + Q_w^{1/n} - 0.33(Q_s Q_w)^{1/2n}\right]^n \tag{3}$$

Both Q_s and Q_w depend, in part, on the building envelope flow coefficient, C, and the flow exponent, n, determined by blower door testing. They are calculated as:

$$Q_s = CF_s\left[\rho g H\left(\frac{T_{in} - T_{out}}{T_{in}}\right)\right]^n \tag{4}$$

$$Q_w = CF_w\left[\frac{\rho}{2}(S_w U)^2\right]^n \tag{5}$$

where
ρ = air density, kg/m^3
g = acceleration due to gravity, m/s^2
H = average height of building at highest eave, m
T = temperatures in K inside (in) and outside (out)
S_w = wind shield factor to account for building microclimate, dimensionless
U = wind speed, m/s
F_s = dimensionless flow factor for stack effect
F_w = dimensionless flow factor for wind effect

The dimensionless flow factors F_s and F_w are calculated based on assumed leakage locations. There is no open flue for this house, so the leakage locations are distributed across the ceiling, walls, and floor. The leakage distribution and the wind shield factor, S_w, were optimized through fitting the relevant coefficients using measured air exchange rates in the house, determined by tracer gas testing as described above.

3.2. Mechanical ventilation

In the previous study an Energy Recovery Ventilator (ERV) was used to provide additional air exchange for the house. The membrane-based core of the ERV transfers both heat and moisture, so the net moisture exchange with outdoors associated with mechanical ventilation depends on the ERV moisture transfer effectiveness as well as on its runtime. In a subsequent study the ERV effectiveness was modeled [35] and the results from that investigation were used to improve the moisture balance modeling that is presented below. Once the radon system was installed the ERV was turned off for the remainder of the study. Prior to the installation of the radon system, the total air exchange was a simple addition of the natural air flow (Q_{aim}) and ERV air flow. But this simple addition does not work for the radon fan since it changes the pressure distribution and leakage areas in the house [36]. When the radon fan was active the total ventilation rate, Q_{total} (m^3/s), was calculated as an addition similar to the method used to add the wind and stack effects in the AIM-2 model, but with different coefficients. The coefficients were picked to match the tracer gas exchange data taken when the radon fan was on, resulting in equation (6).

$$Q_{total} = \left[Q_{aim}^{1/(n-0.4)} + Q_{mech}^{1/(n-0.4)} - (Q_{aim}Q_{mech})^{1/2(n-0.4)}\right]^{(n-0.4)} \quad (6)$$

where Q_{mech} is radon fan air flow (m^3/s).

4. Moisture balance model

4.1. Overview

The moisture balance model used to calculate the moisture infiltration from soil gases is similar to that used in the previous study. The refinements added are addressed after an overview of the method. Essentially, the rate of change in mass of water vapor indoors depends on the rates of multiple moisture flow mechanisms: soil gas infiltration, generation with a humidifier, air exchange with outdoors, vapor diffusion through the building envelope, and sorption and condensation. These moisture flow terms are illustrated in Fig. 2 and laid out in equation (7).

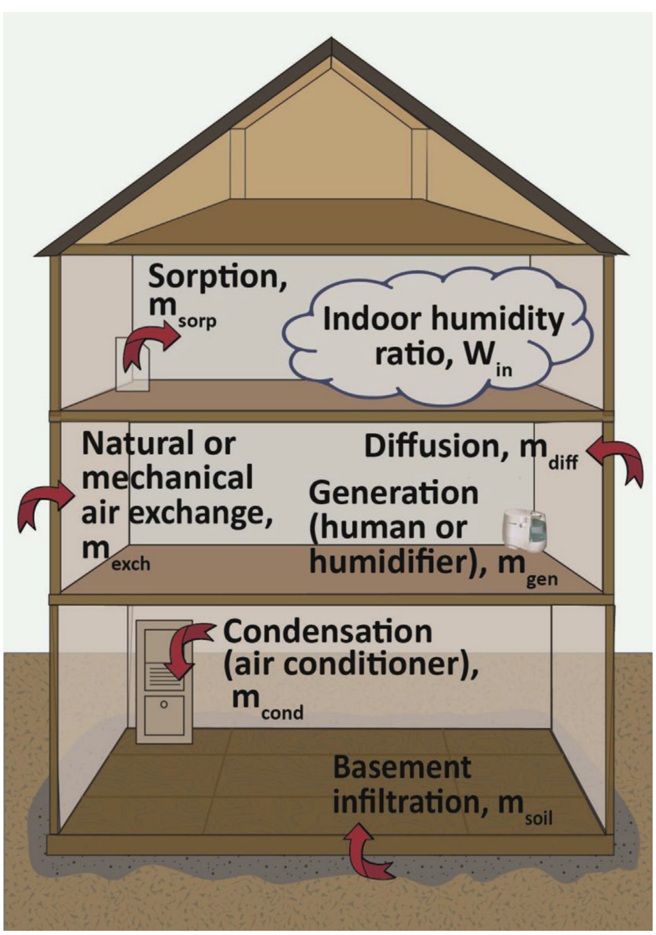

Fig. 2. Moisture balance terms.

$$\rho V \frac{dw_{in}}{dt} = m_{soil} + m_{gen} + m_{exch} + m_{diff} + m_{sorp} + m_{cond} \quad (7)$$

where

ρ = indoor air density, kg/m^3

V = volume of house, m^3

w_{in} = indoor humidity ratio indoor air, kg water vapor per kg dry air

t = time, s

m_{soil} = rate of moisture transport into basement from soil gas infiltration, kg/s

m_{gen} = rate of moisture added through humidification, kg/s

m_{exch} = rate of moisture added through exchange with outdoor air, kg/s

m_{diff} = rate of moisture added through diffusion, kg/s

m_{sorp} = rate of moisture added through sorption, kg/s

m_{cond} = rate of moisture lost[2] through condensation on cold surface, kg/s

The mass rate of change in the indoor humidity ratio is approximated numerically for a 1 h time step Δt as

$$\frac{dw_{in}}{dt} \approx \frac{w_{in}^{t} - w_{in}^{t-1}}{\Delta t} \quad (8)$$

where w_{in}^{t} and w_{in}^{t-1} are the indoor humidity ratios for the current and previous hours, respectively. The indoor humidity ratio and all mass flow rates in equation (7), which are time dependent, are approximated numerically using a single value for each hour. The moisture infiltration results presented later are calculated using this moisture balance by measuring or calculating all the other moisture terms in equation (7) and using the conservation of mass to infer the basement infiltration.

4.2. Humidification

In a typical house the humidification term could be significant and would account for moisture added to the air through human activities like breathing, cooking, and showering. No one lives in the research and demonstration house monitored for this study, but humidifiers were used for a few days in order to test the impact of wood sorption on indoor RH and provide data to calibrate the sorption model discussed below. During those days two humidifiers were charged and run continuously, injecting water vapor into the basement air. One of the humidifiers was placed on a scale with an automated program recording the total mass each minute. The average mass loss rate was calculated and double that rate was used as the rate of humidification to account for the two humidifiers. Otherwise, when the humidifiers were not running, the humidification rate was set to zero.

4.3. Moisture addition by air exchange

4.3.1. Natural infiltration and soil gas exhaust ventilation

When the radon fan was running, the moisture addition rate associated with air exchange was calculated using equation (9) and the air flow rate predicted by equation (6), Q_{total}.

$$m_{exch} = Q_{total}\left(\frac{P_{out} - P_{in}}{R_w T_{in}}\right) \quad (9)$$

where

R_w = gas constant for water vapor, 461.5 J/kg K

[2] Moisture lost is a negative number in this moisture balance.

P = vapor pressure of water (Pa) at interior (in) and exterior (out)

When the radon fan was off equation (9) was used with air flow rate Q_{aim} rather than Q_{total}.

Note that equation (9) assumes all the air exchange is between indoor and outdoor air. The situation is actually more complicated; the details of air flow through different parts of the house are not captured by this one equation. For example, in winter with the radon fan off, air exits the house near the top but enters near the bottom; the proportion of infiltrating air that comes in from below grade is not accounted for in the equation, and the actual vapor pressure of incoming air is likely to be higher than outdoors due to soil moisture. But these complications are handled by including m_{soil} in the full moisture balance, without having to know or measure the vapor pressure of water in the soil gas or the proportion of the total air flow that is influenced by the soil gas.

4.3.2. Energy recovery ventilation

When the ERV was running, m_{exch} was calculated as the sum of two terms. The moisture addition rate due to natural air exchange, m_{na}, was calculated using the form of equation (9) substituting Q_{aim} for Q_{total}. Then the moisture addition rate due to mechanical ventilation, m_{mech}, was calculated based on the performance of the ERV core. A brief overview of ERV performance is outlined here following the analysis of Barringer and McCugan [37] and using the 4 ports as numbered in Fig. 3, so that port 1 is the outside incoming air, 2 is the supply air to the house, 3 is the return air going into the ERV for exhaust, and 4 is the exhaust air exiting the house.

Under this numbering scheme a mass balance in the core requires

$$w_1 m_1 + w_3 m_3 = w_2 m_2 + w_4 m_4 \tag{10}$$

The various m subscripts are mass flow of dry air through the various ports, and w is the humidity ratio. The ERV moisture transfer effectiveness, ε_m, is defined as

$$\varepsilon_m = \frac{w_2 - w_1}{w_3 - w_1} \tag{11}$$

which reflects the total moisture transfer to supply air compared to total moisture difference between indoor and outdoor. Next it was assumed that the ERV airflows were balanced, as was the case in this study, so that all the dry air mass flow rates, m_{da}, through the various ports of the ERV were equal. Hence the moisture addition rate was calculated as

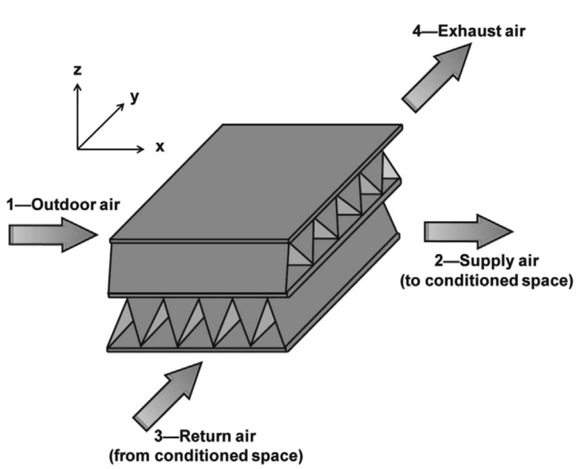

Fig. 3. ERV core air flow port labeling scheme.

$$m_{mech} = m_{da}(w_2 - w_3) = m_{da}(w_1 - w_3)(1 - \varepsilon_m) \tag{12}$$

Finally, ε_m, was calculated based on the results of Boardman and Glass [35]

$$\varepsilon_m = \alpha h + \beta h^2 + \gamma\theta\Big(h - 1\Big) \tag{13}$$

where the empirical fit parameters are $\alpha = 1.464$, $\beta = -0.836$, $\gamma = 0.01692\ ^{\circ}C^{-1}$, θ is the average temperature in °C, and h is the average relative humidity ($h = 1$ at 100% RH). The averages are taken between indoor and outdoor conditions.

4.4. Diffusion through building envelope

In many houses water vapor diffusion can be neglected as insignificant in comparison to air exchange [16]. Vapor diffusion was not neglected for this study, however, because the exterior walls of the research and demonstration house were vapor-open, and moisture was known to accumulate in the cellulose insulation and the oriented strand board (OSB) sheathing during the winter [29]. Instead the calculation was done following the method in the previous study [6] where a one-dimensional WUFI model was created to estimate the diffusion through the above-grade walls and calibrated through comparison with the measured moisture content of the OSB sheathing. Diffusion through the ceiling was neglected since it has a polyethylene vapor barrier. Any remaining diffusion from the basement is lumped into the m_{soil} term. For this study the same wall configuration and properties previously validated was used again, but updated with the indoor and outdoor boundary conditions for the time period of this study, from July 2011 to August 2012.

The modeled wall, from inside to outside, consisted of interior latex paint[3] on 12.5 mm gypsum board, 140 mm cellulose fiber insulation, 12 mm OSB sheathing, a polyolefin weather barrier, a 30 mm air gap, and a brick veneer cladding. The air gap was modeled with an air change source of 2.2 ach with outside air. The hourly moisture flux at the gypsum wall surface scaled by the total wall area was used as m_{diff} in the moisture balance. The indoor and outdoor boundary conditions were taken from the previously mentioned temperature, humidity, and wind sensors. Rainfall was taken from the KMSN (local airport) weather station, and solar irradiance from the ISIS Network MSN station [38].

4.5. Moisture sorption

Sorption was calculated using empirical sorption constants, k (kg/s m^2), following the method of TenWolde [39] and similar to the previous study. However, for this study, both a short-term and a long term constant were included similar to work done by Plathner et al. [40].

$$m_{sorp} = k_{short}A(RH_{ws} - RH) + k_{long}A(RH_{wl} - RH) \tag{14}$$

where

A = total floor area of the building (m^2)

RH = current indoor relative humidity, %

RH_{ws} = short-term exponentially weighted average of previous indoor relative humidity

RH_{wl} = long term exponentially weighted average of previous indoor relative humidity

This method of handling sorption accounts for both the short and long term storage in hygroscopic materials which depends on

[3] The water vapor diffusion resistance factor was 200 for a 1 mm thick layer.

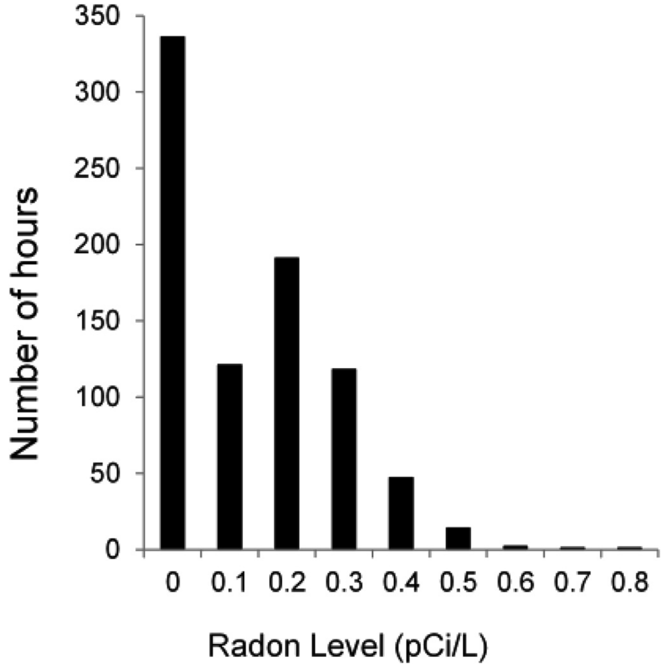

Fig. 4. Outdoor radon levels.

the RH history of the material. The RH was used rather than the vapor pressure in this model for simplicity following the argument of Tenwolde [41] that the storage materials' moisture content attains equilibrium with a time-averaged RH. Further, the RH and vapor pressure are closely related since the indoor temperature was well controlled. The k values were determined experimentally following the method of TenWolde [39] in which the sorption constant is tuned to allow predicted RH to match the actual RH, given a known RH history, known air exchange, and approximate moisture generation. For the short term test a humidifier added bursts of moisture to the air over a short (8 h–1 day) period, creating an oscillation in the room RH. For the long term test the humidifiers were run close to continuously for a month creating a sustained increase in RH.

4.6. Condensation

The only significant condensation in this house occurs during the summer as a result of the dehumidifying effect of the air conditioner. The condensate was captured and run through a tipping bucket (Rainwise RainLog system) before flowing to the drain. Each tip of the bucket was recorded and data was taken from the logger periodically and processed to produce hourly values for moisture removed from the air. Wintertime condensation was not observed on any windows or interior surfaces during this study.

5. Results

5.1. Radon levels

The radon report which initiated this study showed an average of 8.7 pCi/L in the basement of the test house during the winter. This number can be compared to the background value recorded outdoors and the indoor level when the radon fan is turned on and off. Fig. 4 plots a histogram of hourly readings from the RS300 from selected days in summer and early fall. The average of the 830 values is 0.14 pCi/L with a standard deviation of 0.14.

During August 2011 the RS300 was moved inside to compare with the RS800. Fig. 5(a) shows that both instruments agree on the radon level which rises when the fan is turned off and falls when the fan is turned back on.

Fig. 5(b) shows the basement to outdoor pressure difference during the same time period. Negative numbers in the graph indicate the basement is under negative pressure with respect to the outside. There was no monitoring of the basement pressure relative to the soil, although large negative pressures compared to the outside could be expected to overpower the negative pressure field across the floor at spots far away from the PVC pipe. The measured pressure differences are discussed in detail below. The

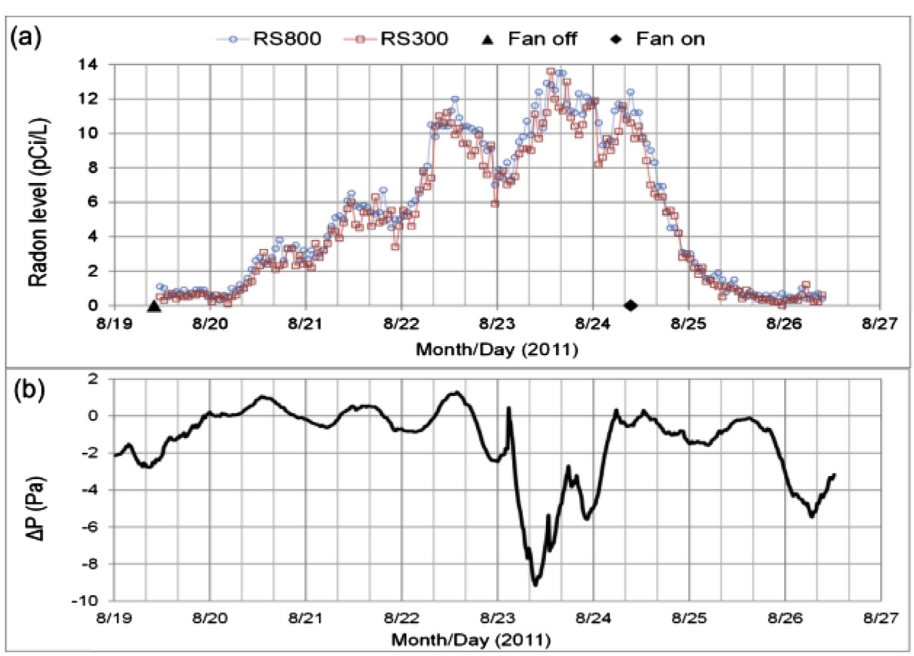

Fig. 5. Indoor radon level with fan off and fan on periods (a) and basement-outdoor pressure difference (b).

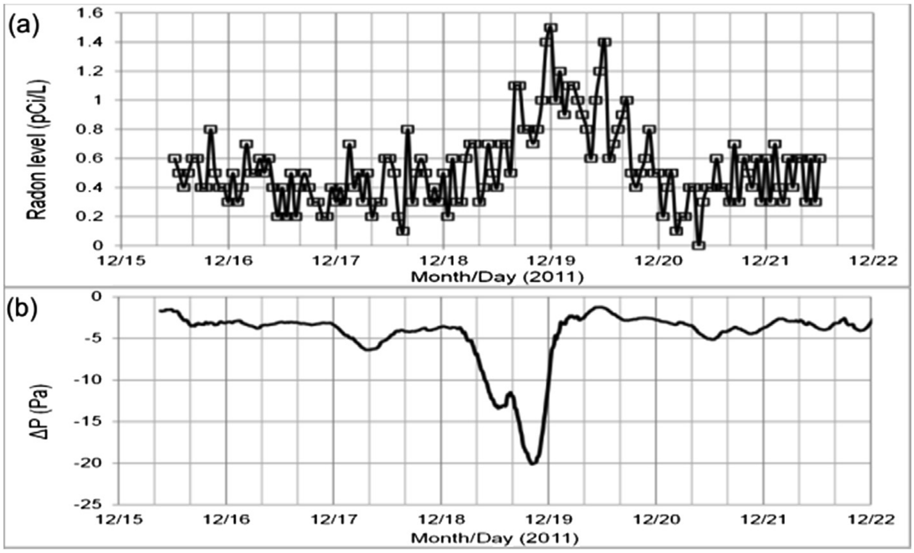

Fig. 6. Indoor radon level with fan on (a) and basement-outdoor pressure difference (b).

main point of Fig. 5(a) is to show that the radon fan controlled the indoor radon levels, reducing the radon levels from near 10 pCi/L on 8/24 to below 2 pCi/L one day after being turned on. Further, for the period 9/2/11 to 9/8/11 during which the radon fan was continuously on, the average radon level was 0.4 ± 0.3 pCi/L (one standard deviation). Similarly for the period 4/6/12 to 4/13/12 with the fan on the average radon level was 0.3 ± 0.2 pCi/L.

Fig. 6(a) again shows the indoor radon level with the fan continuously on as was typically the case. Even with the fan on the radon level can rise somewhat above the typical outdoor level of 0.14 pCi/L and average indoor level near 0.4 pCi/L. For example, on 12/19 a wind induced pressure drop shown in Fig. 6(b) results in a corresponding spike in indoor radon levels. From 12/16/11 to 12/18/11 noon the radon level was 0.4 ± 0.2 pCi/L but rose to 1.4 pCi/L on 12/19 right after the large pressure drop late in the day on 12/18/11.

Finally, Fig. 7(a) shows that the radon level did not always rise above 10 pCi/L when the fan was turned off, and could reach levels near outdoor conditions even with the fan off. Thus within 1 day of the fan being turned off the indoor radon level rose above 2 pCi/L but never higher than 4 pCi/L during all the time the fan was off.

5.2. Pressure differences

It is useful to review the outdoor-basement pressure difference readings, taken every 15 min, at two time scales. First, looking over the whole year from summer to summer, Fig. 8 plots a condensed view of the full year's data. The thin line 1 day moving average was created by smoothing the individual data points and then plotting only the 1 day moving average. The thicker curve is a simple second-order polynomial fit to that data illustrating the drop in

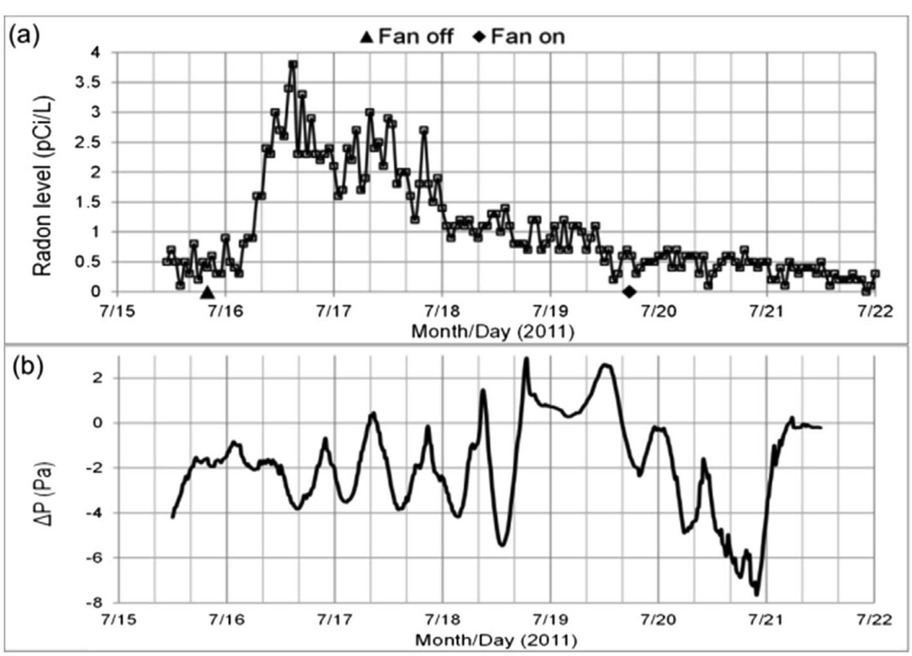

Fig. 7. Indoor radon level with fan off and fan on periods (a) and basement-outdoor pressure difference (b).

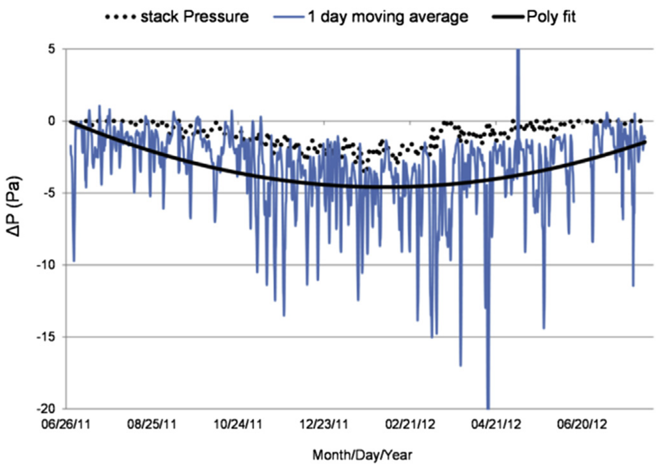

Fig. 8. Full year pressure difference outside to basement.

pressure during the winter. For comparison Fig. 8 also plots as a dotted line the stack pressure calculated from the average daily indoor–outdoor temperature difference assuming a height 2.7 m from the neutral plane, which is typically a point near the basement floor. Again, negative numbers in the graph indicate the basement is under negative pressure with respect to the outside during the winter. Most prominent in Fig. 8 are the spikes that result from wind pressure, which can dominate the stack effect for extended periods, but the main trend as illustrated in the Poly fit follows the stack pressure.

Second, looking over the time period of 7–10 days shows that short-term pressure events sometimes correlate with indoor radon levels. For example, Fig. 7(b) plots the pressure during July days that correspond to the radon readings in Fig. 7(a). The radon levels are generally low, below 4 pCi/L, and decline to 1 pCi/L on 7/19 during the time that the basement pressure is low and even attains positive pressure with respect to outdoors on 7/19, before the radon exhaust fan is turned on. All these radon levels are below the long term average of over 8 pCi/L when the radon fan is off. Although this could be due to variability of the radon source strength, we know the driving pressures for convective transport were low; indoor and outdoor temperatures were roughly the same so there was no stack effect, and the pressure readings showed little wind activity during this time. Contrast the radon data in Fig. 7(a) with a similar time period later in the same summer from Fig. 5(a). During these August days the stack effect was again negligible, but the radon level rose to 14 pCi/L, well above the long term average. This radon peak occurred just a few hours after the large wind event seen in Fig. 7(b) on 8/23. This suggests that convective transport driven by wind is significant for driving radon entry, as was also found by previous studies.

Finally, even when the radon fan was running, wind events correlated with radon level changes. As illustrated in Fig. 6(b), a significant negative basement pressure during the winter coincided with the modest radon level rise in Fig. 6(a). The wind pressure here was twice as much as we have seen in the summer snapshots. It took significantly more wind to overcome the radon fan negative pressure, but the radon level rose to three times its normal background during this episode.

5.3. *Air exchange model calibration*

Finding the moisture entry from the soil to the basement is more difficult than measuring the radon entry, which tracks the indoor radon levels. But like radon, moisture entry is strongly influenced

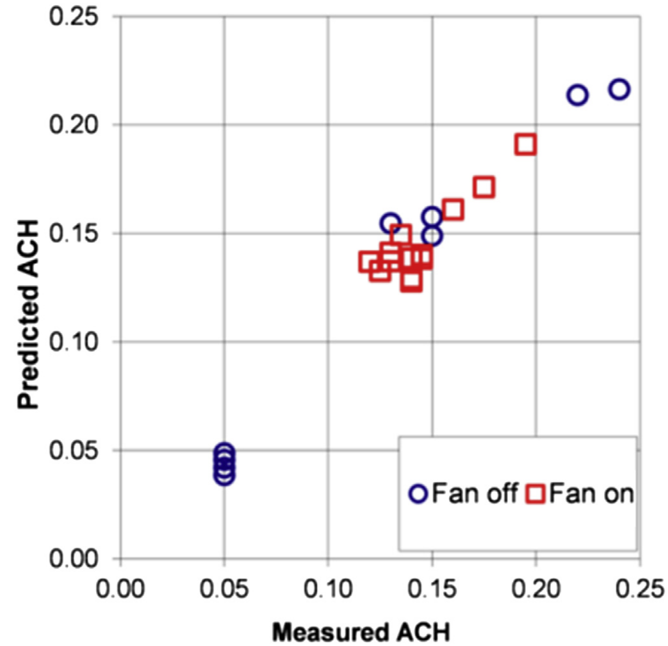

Fig. 9. Predicted ACH from AIM-2 versus ACH measured by tracer gas decay.

by pressure differences across the basement floor. The AIM-2 model, which accounts for both stack and wind effects on external air exchange, was a key component in the moisture balance model which allowed measurement of moisture entry. The most basic components of that model are the C and n factors that come from blower door measurements. In the previous study C[4] was 0.0503 $m^3/s\ (Pa)^{-n}$ with $n = 0.679$. For this study eight additional blower door tests were performed, most of which had a higher n factor, so n was initially set to 0.7. The final AIM-2 optimized values were $C = 0.0438$ and $n = 0.701$.

The optimization process involved calculating Q_{aim} and Q_{total} using equation (3) through (6) and comparing the result to the measured air leakage. Tracer gas tests were run on 23 different days across a variety of seasons and wind conditions with the radon fan both on and off. The optimization minimized the sum of the squares of the differences between the predicted and measured values. This resulted in a radon fan flow of 0.0316 m^3/s (67 cfm) added to the natural infiltration flow using equation (6) to obtain Q_{total} when the fan was on. Under both conditions there were roughly equal leakage percentages across the floor, walls, and ceiling. The wind shield factor S_w was 0.55. Fig. 9 shows the success of the optimization by plotting the predicted air exchange rate in air changes per hour (ACH) against the measured ACH. Perfect prediction would result in all data points on a diagonal line in Fig. 9. The actual RMSE was 0.03 ACH with a maximum deviation of 0.08 ACH.

5.4. *Moisture infiltration*

So, using the AIM-2 model for air exchange calculations, along with the rest of the moisture balance, the soil moisture infiltration into the basement can be estimated. Fig. 10 shows results from the earlier study for a whole year, but with the results updated to reflect a better calculation of moisture transfer effectiveness in the ERV core and revised sorption calculations discussed later.

[4] C is often given in units of cubic feet per minute (cfm)/Pa^n; 0.0503 $m^3/s\ Pa^n$ is 106.6 cfm/Pa^n.

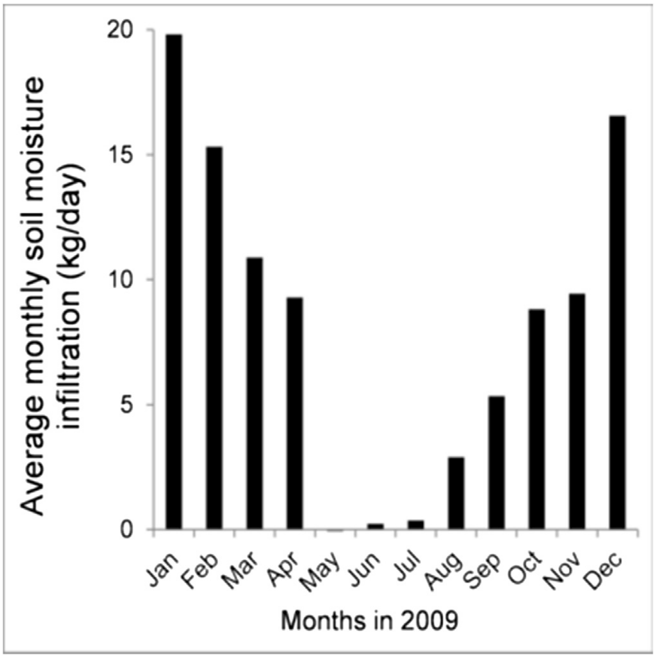

Fig. 10. Soil moisture infiltration for a full year with no radon fan.

First note that during the winter the foundation is a significant source of moisture for this house, over 15 kg/day for winter months of January, February, and December 2009. In the previous study [6] these results were shown to be dominated by the stack effect which is correlated with the large soil moisture infiltration during the winter. That paper argued there was always adequate soil moisture available to enter the house by convective transport. The alternative hypothesis that the soil moisture changes seasonally, perhaps reduced in the summer, was judged less likely since there was no seasonal variation in the moisture content of the bottom plates of the foundation. Bottom plates were chronically damp, varying spatially from about 20% MC on the "downhill" side of the building to about 40% MC on the "uphill" side of the building.

This stack effect correlation is here illustrated in Fig. 11 by plotting a simple prediction based on indoor to outdoor temperature difference in equation (15) versus the full calculation of soil moisture infiltration from equation (7).

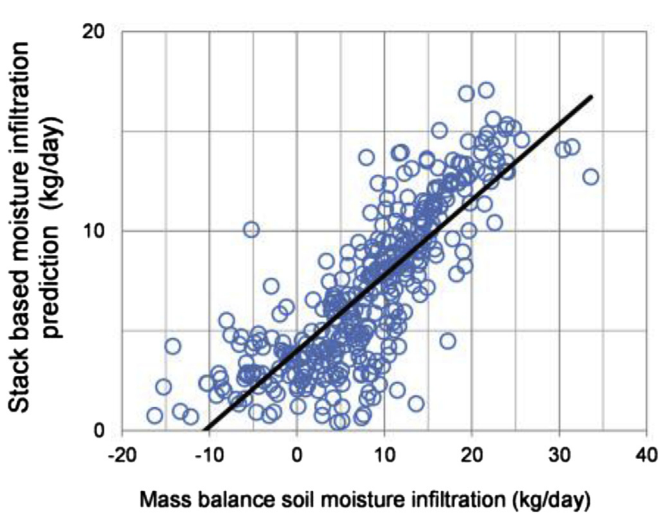

Fig. 11. Daily soil moisture infiltration calculated from equation (15) versus equation (7).

$$m_{pred} = k_{soil}\left(\frac{T_{in} - T_{out}}{T_{in}}\right)^{0.7} \tag{15}$$

Equation (15) is similar to equation (4) of the AIM-2 model with the temperatures in Kelvin. When the outdoor temperature was higher than indoor temperature, m_{pred} was set to zero. The value of k_{soil} was set based on optimizations used to estimate the sorption constants discussed later. That optimization process required an estimate of the soil moisture infiltration. The value of k_{soil} was set to allow the sorption model to best predict indoor relative humidity when the radon fan was off.

This earlier result can be contrasted with measurements from this study after the radon mitigation system was in place. During another full year there was much less soil moisture infiltration when the radon fan was on. Fig. 12 illustrates this by showing the monthly average infiltration both with the fan on, as was typical, and for the hours when the fan was off.

No data were available with the fan off after March 2012. Note that the outdoor winter temperatures driving the stack effect were generally milder for 2011–12 (average −1.5 °C from Dec through Feb) than in 2009 (average −7.3 °C for months Jan, Feb, Dec), so the expected soil moisture infiltration would be less for Fig. 12 compared to Fig. 10. Nevertheless, the estimated soil moisture infiltration was low for most of the study. The average for all days with the radon fan on was only 2.1 kg/day, and always below 4 kg/day during the winter months for a reduction of over 10 kg/day during winter. In the previous study the uncertainty in daily moisture infiltration was estimated to be ±3 kg/day during winter. A more detailed uncertainty estimate for this study will be presented later in the discussion, but clearly turning on the radon fan significantly reduced the soil moisture infiltration, validating the moisture balance model.

5.5. Moisture sorption

Built into the moisture balance, and hence into the results in Figs. 10 and 12, is an estimate of the moisture exchange between the air and the wood in the basement due to sorption. In the previous study there was only one sorption term k, with a value of 0.0972×10^{-6} kg/s m^2. The exponentially weighted time average went back 40 h, with a time constant of 10 h. In this study k_{short} was 0.0953×10^{-6} kg/s m^2 and the short weighted time average went back only 36 h, but the time constant was 72 h. In addition k_{long} was 0.0152×10^{-6} kg/s m^2 and the long weighted time average went back 552 h, excluding the most recent 24 h with a time constant of 1104 h. Before presenting the relative humidity (RH) data that informs these results the exponentially weighted average is presented in more detail.

The basic premise of the sorption model is that the moisture transfer with the house furnishings (sorption) depends on the difference between the RH of the air and the surface moisture content of the furnishing. Further, the furnishings' surface moisture content depends on the RH history of the house. Finally, the exponential average is used because the most recent RH history is most relevant for understanding the surface moisture content. The weighted average was calculated:

$$RH_w = \sum_{j=1}^{\tau} RH(j + start) \times W(j,\tau) \Bigg/ \sum_{j=1}^{\tau} W(j,\tau) \tag{18}$$

Here, the RH function returns the RH at a time step j hours earlier than current RH and the offset start is used in the long calculation to begin the RH average 24 h earlier. The W function applies the exponential factor:

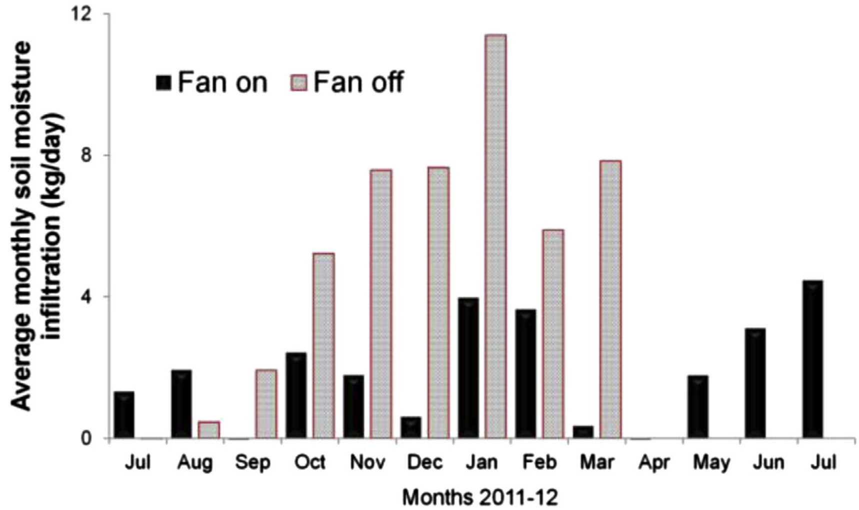

Fig. 12. Soil moisture infiltration when radon fan is mostly on, with similar data for fan off when available.

$$W(j,\tau) = e^{-0.5j/\tau} \tag{19}$$

and τ is the total number of steps (hours) to go back. The selection for the value of τ for the two different length weighted averages requires engineering judgment. Any number of combinations of τ and k could have produced a reasonable fit with the actual RH history. For this study the τ values were optimized through trial and error after review of the wood moisture content data; the values of k were subsequently optimized based on those fixed time scales. The optimization is again to minimize the sum of the squares of the difference between the actual RH of the indoor air and the predicted RH. The predicted RH is calculated by solving the moisture balance equation (7) for RH and using as inputs an estimate of m_{soil} (equation (15)) and a large known quantity of moisture added through m_{gen}. Essentially, k is estimated by charging up the wood in the house through injecting water into the basement air and watching the response of the indoor RH to the balance of water added through humidification and water subtracted due to sorption into the wood. For this study the estimate of m_{soil} was from equation (15) using different k_{soil} values depending on the state of the radon fan.

The exponentially weighted average used for this study is slightly different than that originally used for the previous study in that the exponential drop off is less severe. Given a fixed number of time steps to go back, the current study using equation (19) weights each step more equally, corresponding to a longer decay time constant. This resulted in a better fit, and the more equal weight was applied to the previous data results as presented in Fig. 10, as well as in the current data.

The graph of predicted versus actual RH for the short term test is presented in Fig. 13.

The spikes in indoor RH in late November were caused by turning on and then off humidifiers which added about 8 kg of water over a period near 18 h. The differences evident in the short term prediction and measured values are a result of the estimate for soil moisture infiltration. When using the full moisture balance model (equation (7)) instead of equation (15) the prediction root-mean-square error drops from 2 to 0.35 %RH. The long term k_{long} was estimated through a similar procedure but the

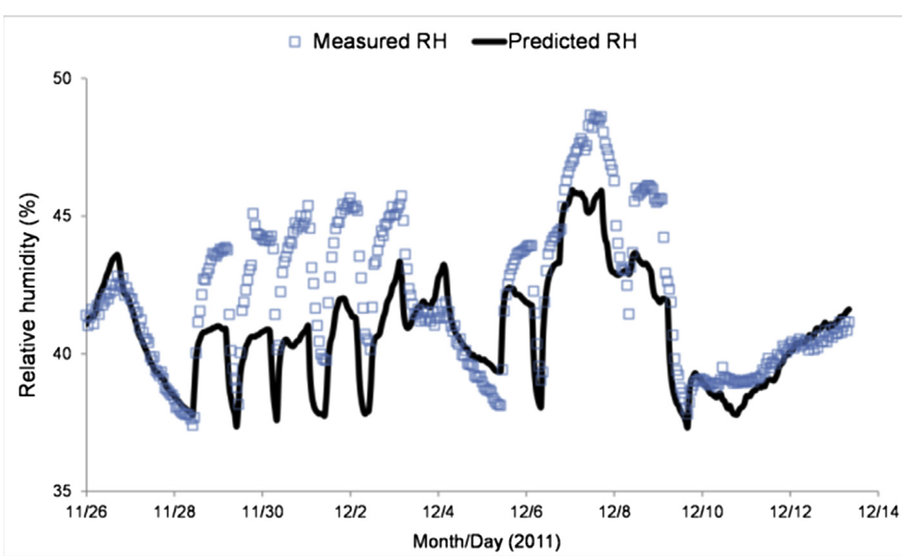

Fig. 13. Measured and predicted RH during short term sorption test.

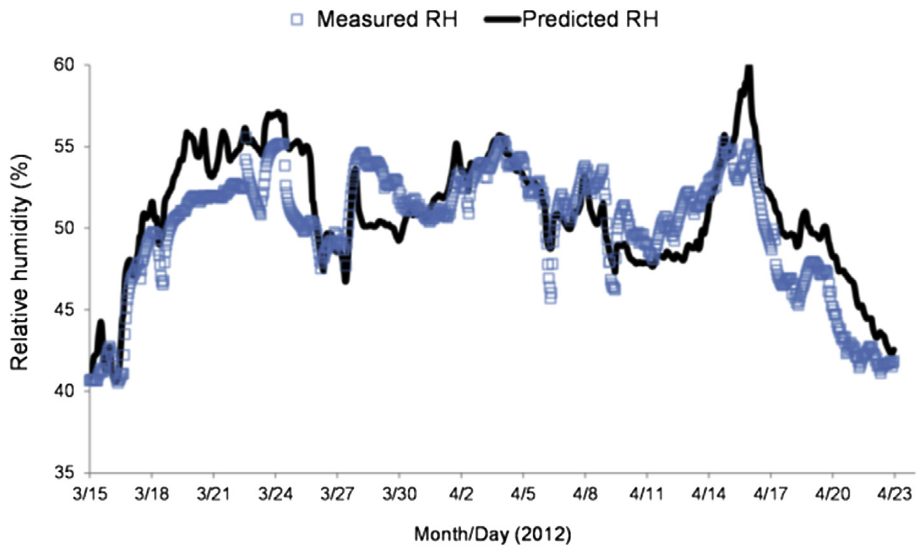

Fig. 14. Measured and predicted RH during long term humidification.

humidifiers ran constantly for over a month adding near 1/3 kg per hour. Fig. 14 shows those results. Again use of the full moisture balance model reduces the root-mean-square error from 2.3 to 0.38 %RH.

The actual moisture content readings from the 2″ × 4″and plywood floor sample points across the whole year are shown in Fig. 15. These data points give direct insight into wood sorption and average RH history of basement. Over the range of indoor RH values in this study (35–60%), equilibrium moisture content of wood varies roughly linearly with RH. Fig. 15 illustrates the seasonal response of wood moisture content; higher RH values in summer correspond with higher wood MC values; lower RH values in winter correspond with lower wood MC.

The short term sorption test did not have any effect on the drying occurring during the early winter of 2011–12, which appears to stop in mid-February 2012. The long term sorption test that started in mid-March did increase the wood moisture content early in the test but wood MC then held steady during the remainder of the extended humidification.

6. Discussion

6.1. Radon

Not surprisingly active soil depressurization was effective in reducing the radon level in the test house, similar to the results of others [7,9,11,42]. This is why it is a standard method recommended by the EPA [3]. Minkin and Shapovalov [43] have been critical of the assumption that pressure driven radon transport is the dominate mechanism for indoor radon entry. The focus of their criticism is mainly on the stack effect as a significant driving force and they advocate for thermodiffusion as an important factor in concrete foundations. This test house has a plywood floor and there is evidence of a pressure driven air flow, but with wind as the mechanism for creating the pressure difference. For example, Fig. 6 illustrates a correlation between increased radon entry and large basement negative pressures, even when the radon fan is on. And when the radon fan is off, Fig. 5 shows a similar correlation. However, despite the evidence that pressure driven flow effects

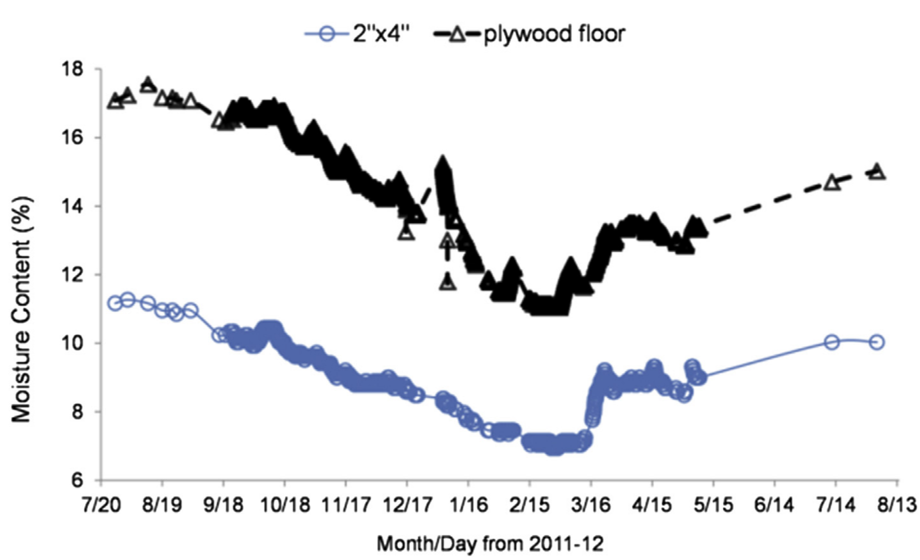

Fig. 15. Wood moisture content trends over the year.

radon gas movement, Figs. 5 and 7 also show that radon enters the basement during the summer without any strong wind pressures and during a time period when the basement pressure is near outdoor levels. So, from August 20 to 22 there was neither stack nor wind effect driving radon entry, yet the level rose to near the long term average radon level measured by alpha track during the winter. There is too little evidence to declare any radon entry mechanism primary in this case study. Many mechanisms appear to be active.

6.2. Moisture

ASD was also effective at reducing soil moisture infiltration. Comparison of Figs. 10 and 12 shows the significant reduction in moisture infiltration during the winter once the radon fan was on. In fact the average daily infiltration calculated when the fan was on was only 2.1 kg/day which is less than the typical uncertainty ±4 kg/day. Overall moisture infiltration uncertainty was dominated by RH measurement uncertainty. The moisture infiltration uncertainty was estimated through a sensitivity analysis on 8 selected days. A bracketing scenario was implemented to calculate the effects of increasing and decreasing moisture exchange through changing the driving terms in the AIM-2 model. At one extreme (to represent a clear over-estimate), the hourly wind speed values were increased by 0.45 m/s, the outdoor temperature was decreased by 0.56 °C, the indoor RH was increased by 1%, and the outdoor RH was decreased by 1%. At the other extreme (to represent a clear underestimate), the wind speed values were decreased by 0.45 m/s, the outdoor temperature was increased by 0.56 °C, the indoor RH was decreased by 1%, and the outdoor RH was increased by 1%. Under these bracketing scenarios the soil moisture infiltration uncertainty was as high as ±5.1 kg/day during the summer and as low as ±3.1 kg/day during the winter. This moisture balance method of estimating soil moisture infiltration cannot resolve small amounts of moisture infiltration due to the difference methodology it uses. However, it is still useful for general estimation of the otherwise difficult to determine soil moisture infiltration, and robust enough to demonstrate the significant reduction (from over 15 kg/day to under 4 kg/day) in moisture infiltration during the winter in the FPL research and demonstration house due to the radon fan soil depressurization.

The sorption k values reported in the results of this study are similar to those reported by Plathner et al. [40] and have the same trend in that there is a stronger coupling for fast sorption. Plathner et al. found a value of $k_{short} = 0.14 \times 10^{-6}$ kg/(s·m^2) while $k_{long} = 0.05 \times 10^{-6}$ kg/(s·m^2). However, the time constants used in this study were much longer than those used by Plathner. Further, there is an advantage in using a sorption term with two k values to capture the effects of the different time scales as reflected in the 35% increase in root-mean-squared error when using only one sorption k value. It is not surprising that the fast sorption coupling is strong in the FPL research and demonstration house given all the exposed wood in the basement.

7. Conclusion

Soil gas entry through the foundation into the living space can introduce significant quantities of pollutants. Moisture and radon infiltration are prominent examples investigated in this study which shows both stack effect and wind pressure effects on soil gas entry. Wind pressure may have been more significant than stack effect for radon entry. Active soil depressurization significantly reduced the infiltration of both moisture and radon, reducing winter soil moisture infiltration by more than 75%, and dropping indoor radon levels from 8 to below 1 pCi/L. Quantification of soil moisture infiltration was achieved with a moisture balance model although measurement errors limit accuracy, particularly for short time periods. Soil moisture infiltration was greatest during winter. Measurements were consistent with stack effect being the dominant driving force for soil moisture infiltration. Moisture sorption effects in interior hygroscopic materials were modeled more accurately with two terms, corresponding to short-term and long term effects, than with one term in the moisture balance. The moisture balance methodology validated in this case study can be used with any type of basement construction.

Acknowledgments

This manuscript was improved by critical comments from Robert Munson, Marshall Begel, and Laura Hasburgh of the USDA Forest Products Laboratory (FPL), and anonymous reviewers. The writers gratefully acknowledge the help of many FPL colleagues during the course of this investigation, including Charlie Carll, Robert Munson, Sam Zelinka, and Anton TenWolde.

Research was funded by the Forest Products Laboratory of the U.S. Forest Service. This research was performed by U.S. government employees on official time and is therefore in the public domain and not subject to copyright.

References

[1] Heinzerling D, Schiavon S, Webster T, Arens E. Indoor environmental quality assessment models: a literature review and proposed weighting and classification scheme. Build Environ 2013;70:210–22.
[2] Namiesnik J, Goreck T, Kozdron-Zabiegal B, Lukasiak J. Indoor air quality (IAQ), pollutants, their sources and concentration levels. Build Environ 1992;27: 339–56.
[3] U.S. Environmental Protection Agency. Engineering issue, indoor air vapor intrusion mitigation approaches. 2008. EPA/600/R-08–115.
[4] Cooke TF. Indoor air pollutants: a literature review. Rev Environ Health 1991;9(3):137–60.
[5] Cheple M, Huelman PH. Why we need to know more about basement moisture. In: Thermal performance of the exterior envelopes of whole buildings VIII international conference. Clearwater Beach Florida: ASHRAE; December, 2001.
[6] Boardman CR, Glass SV, Carll CG. Estimating foundation water vapor release using a simple moisture balance and AIM-2: case study of a contemporary wood-frame house. In: Thermal performance of the exterior envelopes of whole buildings XI international conference. Clearwater Beach, Florida: ASHRAE; December 5–9, 2010.
[7] Prill R, Fisk WJ. Long term performance of radon mitigation systems. Environmental Energy Technologies Division, Indoor Environment Department, Lawrence Berkeley National Laboratory; March 2002. LBNL-50041.
[8] Turk B, Hughes J. Exploratory study of basement moisture during operation of ASD radon control systems. 2008 [Contractor Report to the U.S. Environmental Protection Agency].
[9] Hubbard LM, Bolker BM, Gadsby KJ, Harrje DT, Socolow RH. Investigation of radon entry into dwellings and the effects of selected radon mitigation techniques. 1988. Final Report from Center for Energy and Environmental Studies (Princeton University) to US EPA (Contract Number CR-814673-01-4) and New Jersey Department of Environmental Protections (Purchase Order 25876).
[10] Gadgil AJ. Models of radon entry: a review. 1991. In: Proceedings of the fifth international symposium on natural radiation environment, NRE-V, Salzburg Austria; September 22-29, 1991. Available from: Lawrence Berkeley Laboratory, LBL-31252.
[11] Turk BH, Prill RJ, Fisk WJ, Grimsrud DT, Sextro G. Effectiveness of radon control techniques in fifteen homes. J Air Waste Manag Assoc 1991;41(5): 723–34. http://dx.doi.org/10.1080/10473289.1991.10466873.
[12] Drylov VV, Ferguson CC. Contamination of indoor air by toxic soil vapours: the effects of subfloor ventilation and other protective measures. Build Environ 1998;33(6):331–47.
[13] Keskikuru T, Kokotti H, Lammi S, Kalliokoski P. Effect of various factors on the rate of radon entry into two different types of houses. Build Environ 2001;36: 1091–8.
[14] Yao Y, Pennell KG, Suuberg EM. Simulating the effect of slab features on vapor intrusion of crack entry. Build Environ 2013;59:417–25.
[15] TenWolde A, Walker IS. Interior moisture design loads for residences. In: Performance of the exterior envelopes of whole buildings VIII international conference. Clearwater Beach, Florida: ASHRAE; December 2–7, 2001.

[16] Glass SV, TenWolde A. Review of moisture balance models for residential indoor humidity. In: Proceedings, 12th Canadian conference on building science and technology, 1; 2009. p. 231–45.
[17] Lu X. Estimation of indoor moisture generation rate from measurement in buildings. Build Environ 2003;38:665–75.
[18] Kalamees T, Vinha J, Kurnitski J. Indoor humidity loads and moisture production in lightweight timber-frame detached houses. J Build Phys 2006;29(3):219–46.
[19] Christian JE. Moisture sources. In: Trechsel HR, Bomberg MT, editors. Moisture control in buildings. 2nd ed. West Conshohocken, PA: ASTM International; 2009. p. 103–9.
[20] TenWolde A, Pilon C. The effect of indoor humidity on water vapor release in homes. In: Thermal performance of the exterior envelopes of whole buildings X international conference. Clearwater Beach, Florida: ASHRAE; December 2–7, 2007.
[21] Huang H, Kato S, Hu R, Ishida Y. Development of new indices to assess the contribution of moisture sources to indoor humidity and application to optimization design: proposal of $CRI_{(H)}$ and a transient simulation for the prediction of indoor humidity. Build Environ 2011;46:1817–26.
[22] Li Y, Fazio P, Rao J. An investigation of moisture buffering performance of wood paneling at room level and its buffering effect on a test room. Build Environ 2012;47:205–16.
[23] Ge H, Yang X, Fazio P, Rao J. Influence of moisture load profiles on moisture buffering potential and moisture residuals of three groups of hygroscopic materials. Build Environ 2014;81:162–71.
[24] Turk B, Hughes J. Movement and sources of basement ventilation air and moisture during ASD radon control: additional analysis. 2009. Contractor Report to US EPA under Agreement XA83146010.
[25] El Diasty R, Fazio P, Budaiwi I. The dynamic modelling of air humidity behaviour in a multi-zone space. Build Environ 1993;28:33–51.
[26] Plathner P, Woloszyn M. Interzonal air and moisture transport in a test house: experiment and modelling. Build Environ 2002;37:189–99.
[27] Woloszyn M, Rode C. Whole building heat, air, moisture response, subtask 1: modelling principles and common exercises. International Energy Agency, Executive Committee on Energy Conservation in Buildings and Community Systems; 2008.
[28] Carll CG, Boardman CR, Olson CL. Case study: performance of a house built on a treated wood foundation system in a cold climate. In: Thermal performance of the exterior envelopes of whole buildings XI international conference. Clearwater Beach Florida: ASHRAE; December 5–9, 2010.
[29] Carll CG, TenWolde A, Munson R. Moisture performance of a contemporary wood-frame house operated at design indoor humidity levels. In: Thermal performance of the exterior envelopes of whole buildings X international conference. Clearwater Beach, Florida: ASHRAE; December 2–7, 2007.
[30] ASTM. Designation E779-03. Standard test method for determining air leakage rate by fan pressurization. 2003 [West Conshohocken, PA].
[31] Boardman CR, Glass SV, Carll CG. Moisture meter calibrations for untreated and ACQ-treated southern yellow pine lumber and plywood. J Test Eval 2011;40(1):184–93.
[32] ASTM. Designation E741-00. Standard test method for determining air change in a single zone by means of a tracer gas dilution. 2006 [West Conshohocken, PA].
[33] Walker IS, Wilson DJ. Field validation of algebraic equations for stack and wind driven air infiltration calculations. HVAC&R Res 1998;4(2):119–39.
[34] Wang W, Beausoleil-Morrison I, Reardon J. Evaluation of the Albert air infiltration model using measurements and inter-model comparisons. Build Environ 2009;44:309–18.
[35] Boardman CR, Glass SV. Moisture transfer through the membrane of a cross-flow energy recovery ventilator: measurement and simple data-driven modeling. J Build Phys 2014;38. http://dx.doi.org/10.1177/1744259113506072.
[36] Sherman MH. Superposition in infiltration modeling. Energy Performance of Buildings Group, Indoor Environment Department, Lawrence Berkeley National Laboratory; 1992. LBNL-29116.
[37] Barringer CG, McGugan CA. Investigation of enthalphy residential air-to-air heat exchangers. 1988. Final Report for ASHRAE Research Project RP-544 (Report No. EEE/ESC-88-08).
[38] Hicks BB, DeLuisi JJ, Matt DR. The NOAA integrated surface irradiance study (ISIS): a new surface radiation monitoring program. Bull Am Meteor Soc 1996;77(12):2857–64. http://www.esrl.noaa.gov/gmd/grad/isis/.
[39] Tenwolde A. Ventilation, humidity and condensation in manufactured housed during winter. ASHRAE Trans 1994;100:103–15.
[40] Plathner P, Littler J, Cripps A. Modeling water vapor conditions in dwellings. In: Third international symposium on humidity and moisture, London, UK, 2; 1998. p. 64–72.
[41] Tenwolde A. A mathematical model for indoor humidity during winter. Symposium on air infiltration, ventilation, and moisture transfer. Washington, DC: Building Thermal Envelope Coordinating Council; 1988. p. 3–32.
[42] Henschel DB. Radon reduction techniques for existing detaches houses: technical guidance (third edition) for active soil depressurization systems. 1993. U.S. Environmental Protection Agency EPA/625/R-93/011.
[43] Minkin L, Shapovalov AS. Indoor radon entry: 30 years later. Iran J Radiat Res 2008;6(1):1–6.